Iğdır Üniversitesi Fen Bilimleri Enstitüsü Dergisi, 12(2): 918-932, 2022
Journal of the Institute of Science and Technology, 12(2): 918-932, 2022

ISSN: 2146-0574, eISSN: 2536-4618

Chemistry **DOI:10.21597/jist.1089701**

ResearchArticle

Received: 18.03.2022 **Accepted: 06.04.2022**

Atıf İçin: Korkmaz A, 2022. Synthesis, Characterization, ADMET prediction, and Molecular Docking Studies of Novel Coumarin Sulfonate Derivatives. Iğdır Üniversitesi Fen Bilimleri Enstitüsü Dergisi, 12(2): 918-932.

To Cite: Korkmaz A, 2022. Synthesis, Characterization, ADMET prediction, and Molecular Docking Studies of Novel Coumarin Sulfonate Derivatives. Journal of Institute of Science and Technology, 12(2): 918-932.

Synthesis, Characterization, ADMET prediction, and Molecular Docking Studies of Novel Coumarin Sulfonate Derivatives

Adem Korkmaz[1*]

ABSTRACT: It was depicted that the coumarin sulfonate derivatives were synthesized and reported tyrosinase and pancreatic lipase inhibitory effects *in silico* application. In addition, the coumarin compounds were designed by introducing a sulfonyl group bearing functional groups such as nitro, methoxy, chlorine, methyl, and bearing naphthyl and thiophenyl motifs. The characterizations of the coumarin sulfonate derivatives were carried out utilizing ^{1}H NMR, ^{13}C NMR, and HRMS analyses. Also, pancreatic lipase and tyrosinase inhibitory activities *in silico* application of the coumarin sulfonate compounds were studied using AutoDock Vina and Chimera software. Moreover, the absorption, distribution, metabolism, excretion, and toxicity properties of the coumarin sulfonate derivatives were performed to explore the properties of target compounds using the preADMET program. Overall, these results exhibited that compound **2c** could accomplish as a potential pancreatic lipase inhibitory.

Keywords: Coumarin sulfonate compounds, tyrosinase, pancreatic lipase, molecular docking, ADMET

Adem Korkmaz[1*] (**Orcid ID:** 0000-0002-0345-5794), Faculty of Health Sciences, Muş Alparslan University, Muş 49250 Turkey[1*]

***Corresponding Author:** Adem Korkmaz, e-mail: a.korkmaz@alparslan.edu.tr

INTRODUCTION

Organic compounds bearing the coumarin motif are a class of structure used in many fields such as drug discovery, cosmetics industry, and food industry (Carneiro et al., 2021; Dorababu, 2022). The having such biological properties of coumarin derivatives pointed out the importance of these compounds (Li et al., 2022). Although coumarin motifs were discovered past time, these compounds have been continued interest by researchers (Tolba et al., 2022). An example of these studies recently was reported human cancer activities of fused tricyclic coumarin sulfonate derivatives with effective results (El-Gamal et al., 2014). Also, the coumarin scaffolds have been used on structure-activity relationships in anti-HIV studies (Xu et al., 2021). In addition, coumarin sulphonate derivatives were reported as alkaline phosphatase inhibition (Iqbal et al., 2018). In another study, sulfonate derivatives bearing coumarin fragments were investigated for their reactive oxygen species (ROS) inhibitory effect (Salar et al., 2018).

Enzymes are important objectives for ordered metabolism. So, enzyme inhibition studies are a vital route to treating metabolic disorders (Bursal et al., 2021; Buldurun et al., 2020; Turkan et al., 2019; Taslimi et al., 2019; Cetin et al., 2021a; Cetin et al., 2021b). Furthermore, tyrosinase and pancreatic lipase activity require to be controlled at particular levels to avoid the destructive conclusions of extreme melanin production. Various synthesized novel compounds for tyrosinase inhibitors have been still investigated but it should not be forgotten that side effects have existed (Korkmaz and Bursal, 2022a; Korkmaz and Bursal, 2022b). Tyrosinase inhibitors of synthetic compounds like arbutin, kojic acid, and hydroquinone have been still discussed as safe from a biosafety point of view due to their side effects. In this context, investigating effective tyrosinase inhibitors with fewer side effects has been still scanned by researchers (Zhang, et al., 2020). For example, peptides (Hariri, et al., 2020), benzothiazole (Korkmaz and Bursal, 2022a), flavones, (Arroo, et al., 2020), and Schiff bases (Alyar, et al., 2019), were investigated for tyrosinase inhibition effects. Moreover, recently, new compounds containing the coumarin motif fragment have been synthesized and their activities on the tyrosinase enzyme have been investigated (Ashooriha, et al., 2019). Pancreatic lipase is known to be a key enzyme for the treatment of obesity (Huo, et al., 2021). Pancreatic lipase inhibitors, which can reduce the absorption of lipids, are used in the treatment of obesity (Sultana, et al., 2020). Instead of orlistat, which has potent activity as a pancreatic lipase inhibitor, research is still ongoing for new and different inhibitors with fewer side effects.

This paper was evaluated the synthesis of novel coumarin sulfonate derivatives and their efficacy for skin problems and obesity by *in silico* application as inhibitors of tyrosinase and pancreatic lipase. Moreover, drug-likeness, pharmacokinetic and physicochemical properties of the novel coumarin sulfonate derivatives were evaluated by defining ADMET.

MATERIALS AND METHODS

General

The melting points of the compounds were obtained from Thermo scientific. The ^{1}H NMR and ^{13}C NMR spectra were analyzed by Bruker 400 spectrometer. HRMS spectra were analyzed at 6200 series TOF/6500 series Q-TOF B.08.00 (B8058.0, acquisition SW Version). The 7-hydroxy-4-methyl-2*H*-chromen-2-one (99.5%), 4-hydroxy-2*H*-chromen-2-one (98%), 2,5-dichlorobenzenesulfonyl chloride (98%), 2,5-dimethoxybenzenesulfonyl chloride (98%), 2-thiophenylsulfonyl chloride (96%), 4-methyl-5-nitrobenzenesulfonyl chloride (97%), 2-naphthylsulfonyl chloride (99%), 2,4,6-trimethylbenzenesulfonyl chloride (99%), hexane (95%), benzene (99%), *N*,*N*-dimethylformamide

(DMF, 99.8%), 2,4,6-trimethylbenzenesulfonyl chloride (99%), and triethylamine (TEA) (99.5%) were utilized without any purification.

The general synthesis process of the coumarin sulfonate derivatives

The TEA-mediated method was used to synthesize the novel coumarin sulfonate derivatives (Korkmaz and Bursal, 2022a; Korkmaz and Bursal, 2022b). The coumarin substrates (3.425 mmol) and TEA (4.110 mmol) were put into a 150 mL flask. Also, DMF solvent (2.7 mL) was put into the flask. Later, corresponding aryl sulfonyl chloride reagents (3.425 mmol) were added to the reaction vessel. The reaction time was scanned by checked Thin Layer Chromatography. Adding 10 mL of water to the reaction vessel was obtained crude product. The obtained product was filtered and dried with a desiccator. The resulted products were crystallized easily with benzene-hexane solvent (1:6).

2-Oxo-2*H*-chromen-4-yl thiophene-2-sulfonate (1a): Color: White crystal (benzene-hexane (1:6)); yield: 67%; M.p. : 128-129 °C;^{1}H NMR (400 MHz, $CDCl_3$), ppm: 7.96-7.82 (m, 2H), 7.74-7.57 (m, 2H), 7.42-7.29 (m, 2H), 7.26-7.18 (m, 1H), 6.50-6.39 (m, 1H); ^{13}C NMR, (400 MHz, $CDCl_3$), ppm: 160.6 (-C=O), 157.7, 153.4, 136.7, 136.3, 133.5, 133.4, 128.1, 124.6, 123.1, 117.0, 114.8, 104.0; HRMS (ESI) m/z: calculated for $C_{13}H_8O_5S_2$ $[M+ H]^+$= 308.98 found 308.98919

2-Oxo-2*H*-chromen-4-yl 2-methyl-5-nitrobenzenesulfonate (1b): Color: White crystal (benzene-hexane (1:6)); yield: 64%; M.p. : 162-165 °C; ^{1}H NMR (400 MHz, $CDCl_3$), ppm: 8.93 (s, 1H), 8.50 (d, J= 8.2 Hz, 1H), 7.77-7.61 (m, 3H), 7.48-7.31 (m, 2H), 6.26 (s, 1H), 2.92 (s, 3H, C**H$_3$**); ^{13}C NMR, (400 MHz, $CDCl_3$), ppm: 160.1 (-C=O), 157.2, 153.5, 146.2, 146.0, 135.4, 134.5, 133.7, 129.3, 125.5, 124.8, 122.8, 117.2, 114.5, 103.9, 20.8 (**C**CH_3); HRMS (ESI) m/z: calculated for $C_{16}H_{11}NO_7S$ $[M+ H]^+$= 362.03 found 362.03255

2-Oxo-2*H*-chromen-4-yl 2,4,6-trimethylbenzenesulfonate (1c): Color: White crystal (benzene-hexane (1:6)); yield: 68%; M.p. : 141-143 °C; ^{1}H NMR (400 MHz, $CDCl_3$), ppm: 7.78 (d, J=7.7 Hz, 1H), 7.61 (d, J= 7.4 Hz, 1H), 7.40-7.32 (m, 2H), 7.07 (s, 2H), 6.02 (s, 1H), 2.70 (s, 6H, 2 units of C**H$_3$**), 2.37 (s, 3H, C**H$_3$**); ^{13}C NMR, (400 MHz, $CDCl_3$), ppm: 160.8 (-C=O), 158.0, 153.5, 145.2, 140.3, 133.2, 132.4 (2 units of Ar-**C**), 130.2, 124.6, 123.28, 123.29 116.9, 115.1, 102.5, 22.7 (2 units of **C**CH_3), 21.5 (**C**CH_3); HRMS (ESI) m/z: calculated for $C_{18}H_{16}O_5S$ $[M+ H]^+$= 345.07 found 345.07866.

4-Methyl-2-oxo-2*H*-chromen-7-yl 2,4,6-trimethylbenzenesulfonate (2a): Color: White crystal (benzene-hexane (1:6)); yield: 67%; M.p. : 166-167 °C; ^{1}H NMR (400 MHz, $CDCl_3$), ppm: 7.57 (d, J=8.6 Hz, 1H), 7.12-7.06 (m, 1H), 7.00 (s, 2H), 6.83 (s, 1H), 6.26 (s, 1H), 2.58 (s, 6H), 2.42 (s, 3H), 2.35 (s, 3H); ^{13}C NMR, (400 MHz, $CDCl_3$), ppm: 160.1 (-C=O), 153.8, 151.8, 151.7, 151.5, 144.5, 140.3, 132.0 (2 units of Ar-**C**), 130.0, 125.7, 118.7 (2 units of Ar-**C**), 114.9, 110.9, 22.7 (2 units of **C**CH_3), 21.1 (**C**CH_3), 18.7 (**C**CH_3); HRMS (ESI) m/z: calculated for $C_{19}H_{18}O_5S$ $[M+ H]^+$= 359.06 found 359.09400.

4-Methyl-2-oxo-2*H*-chromen-7-yl thiophene-2-sulfonate (2b): Color: White crystal (benzene-hexane (1:6)); yield: 59%; M.p. : 156-158 °C; ^{1}H NMR (400 MHz, $CDCl_3$), ppm:7.80 (s, 1H), 7.75-7.59 (m, 2H), 7.16 (s, 2H), 7.04-6.93 (m, 1H), 6.31 (s, 1H), 2.47 (s, 3H, C**H$_3$**); ^{13}C NMR, (400 MHz, $CDCl_3$), ppm: 160.0 (-C=O), 153.9, 151.6, 151.4, 135.8, 135.2, 134.0, 127.8, 125.8, 119.1, 118.7, 115.3, 110.8, 18.7 (**C**CH_3); HRMS (ESI) m/z: calculated for $C_{14}H_{10}O_5S_2$ $[M+ H]^+$= 323.00 found 323.00346

4-Methyl-2-oxo-2*H*-chromen-7-yl naphthalene-2-sulfonate (2c): Color: White crystal (benzene-hexane (1:6)); yield: 80%; M.p. : 156-157 °C; ^{1}H NMR (400 MHz, $CDCl_3$), ppm: 8.42 (s, 1H), 8.12-7.85 (m, 4H), 7.83-7.63 (m, 2H), 7.54 (d, J=8.7 Hz, 1H), 7.09 (d, *J*=8.7 Hz, 1H), 6.94 (s, 1H), 6.26 (s, 1H), 2.40 (s, 3H, C**H$_3$**); ^{13}C NMR, (400 MHz, $CDCl_3$), ppm: 160.0 (-C=O), 153.9, 151.6, 151.55,

151.50, 135.6, 131.8, 130.6, 129.97, 129.92, 129.5, 128.1, 125.79, 125.75, 122.5, 118.9, 118.6, 115.1, 110.9, 18.7 (**C**CH_3); HRMS (ESI) m/z: calculated for $C_{20}H_{14}O_5S$ $[M+H]^+$= 367.06 found 367.06274

4-Methyl-2-oxo-2*H*-chromen-7-yl 2,5-dichlorobenzenesulfonate (2d): Color: White crystal (benzene-hexane (1:6)); yield: 69%; M.p. : 180-181 °C; ^{1}H NMR (400 MHz, $CDCl_3$), ppm: 7.93 (s, 1H), 7.65-7.59 (m, 3H), 7.21 (dd, J=8.7, J=2.3 Hz, 1H), 7.07 (d, J=2.2 Hz, 1H), 6.30 (s, 1H), 2.43 (s, 3H, C**H$_3$**); ^{13}C NMR, (400 MHz, $CDCl_3$), ppm: 159.8 (-C=O), 154.0, 151.6, 150.8, 135.6, 134.3, 133.5, 133.4, 132.0, 131.5, 126.0, 119,3, 118.3, 115.3, 110.6, 18.9 (**C**CH_3); HRMS (ESI) m/z: calculated for $C_{16}H_{10}Cl_2O_5S$ $[M+H]^+$= 384.96 found 384.96961.

4-Methyl-2-oxo-2*H*-chromen-7-yl 2,5-dimethoxybenzenesulfonate (2e): Color: White crystal (benzene-hexane (1:6)); yield: 59%; M.p. : 145-147°C; ^{1}H NMR (400 MHz, $CDCl_3$), ppm: 7.58 (d, J=8.6 Hz, 1H), 7.32 (s, 1H), 7.26-7.16 (m, 2H), 7.12-6.99 (m, 2H), 6.28 (s, 1H), 4.00 (s, 3H, OC**H$_3$**), 3.77 (s, 3H, OC**H$_3$**), 2.43 (s, 3H, C**H$_3$**); ^{13}C NMR, (400 MHz, $CDCl_3$), ppm: 160.1(-C=O), 153.9, 152.93, 151.8, 151.7, 125.6, 123.0, 122.7, 118.8, 118.6, 115.94, 115.93, 115.0, 114.16, 110.72, 56.9 (O**C**H_3), 56.0 (O**C**H_3), 18.7 (**C**H_3); HRMS (ESI) m/z: calculated for $C_{18}H_{16}O_7S$ $[M+H]^+$= 377.06 found 377.06817.

Molecular docking

Molecular docking studies were implemented based on the processing published by us (Korkmaz and Bursal, 2022a; Korkmaz and Bursal, 2022b). UCSF Chimera, AutoDock Vina, Avogadro software, Biovia Discovery Studio Visualizer, and PyMOL visualization software have utilized the process (Trott and Olson, 2009; Pettersen, et al., 2004; Hanwell et al., 2012; Biovia, 2021; Schrödinger, 2021). The binding pocket coordinates with tyrosinase and pancreatic lipase were performed as center x,y,z: -7.59, 46.56, 84.98 / Size x,y,z: 11.00, 11.00, 11.00 and as center x,y,z: 54.73, 46.87, 122.10 / size x,y,z: 14, 14, 14 respectively.

Prediction ADMET studies

ADME, physicochemical properties, drug-likeness, and toxicity prediction of the coumarin sulfonate compounds were employed by using PreADMET and Molinspiration software (Lee, et al., 2017; Molinspiration, 2011).

RESULTS AND DISCUSSION

Chemistry

Coumarin sulfonate derivatives were carried out utilizing 4-hydroxy-2*H*-chromen-2-one and 7-hydroxy-4-methyl-2*H*-chromen-2-one with various functional aryl sulfonyl chloride reagents. In our previous studies, various bases were used for the synthesis of sulfonated derivatives (Korkmaz and Bursal, 2022a; Korkmaz and Bursal, 2022b). For example, 1,5-diazabicyclo[4.3.0]non-5-ene, TEA, *N*,*N*-diisopropylethylamine, potassium tert-butoxide, and 1,8-diazabicyclo[5.4.0]undec-7-ene. As a result of our previous studies, TEA was found to be a more appropriate base in the reaction. In this context, TEA was used for the synthesis of coumarin sulfonate derivatives. The best reaction conditions were obtained at 0-5 °C, 70 min, and 1.2 TEA stoichiometric ratio.

Target coumarin sulfonate derivatives bearing both electron-withdrawing (such as chloride) and electron-donating substituents (Such as methoxy and methyl) were synthesized under mild reaction conditions (Scheme 1). Moreover, thiophenyl and naphthyl motifs have been achieved to integrate into target coumarin sulfonate derivatives.

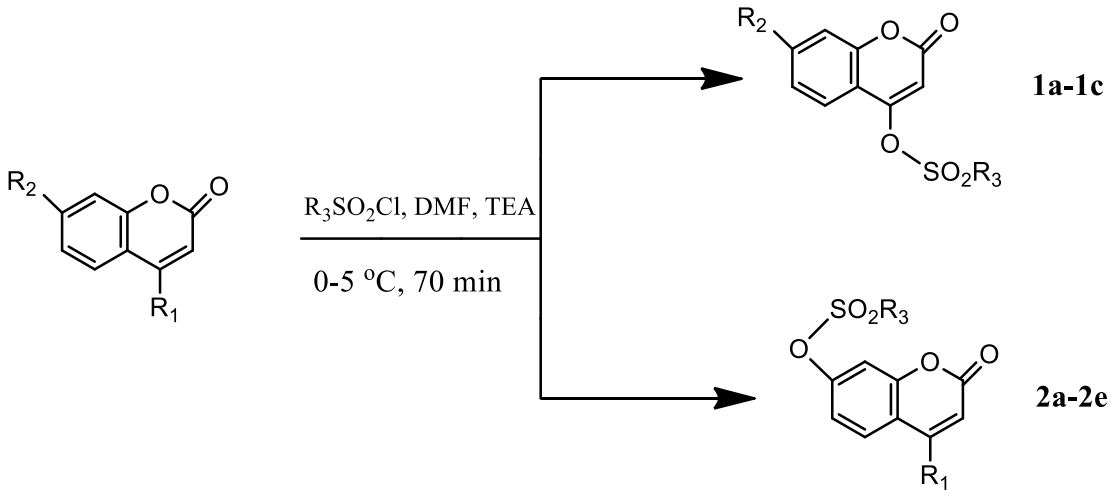

	R_1	R_2	R_3
1a	OH	H	2-Thiophenyl
1b	OH	H	2-Me-5-$NO_2C_6H_3$
1c	OH	H	2,4,6-$(Me)_3C_6H_2$
2a	Me	OH	2,4,6-$(Me)_3C_6H_2$
2b	Me	OH	2-Thiophenyl
2c	Me	OH	2-Naphthyl
2d	Me	OH	2,5-$(Cl)_2C_6H_3$
2e	Me	OH	2,5-$(MeO)_2C_6H_3$

Scheme 1. Synthetic route of synthesized **1a-1c** and **2a-2e**

The obtained coumarin derivatives were characterized by utilizing spectra (^{1}H NMR, ^{13}C NMR, and HRMS). According to ^{13}C NMR spectra, the carbonyl carbon peaks (-C=O) of the target compounds (**1a-1c** and **2a-2e**) were observed as 160.6, 160.1, 160.8, 160.1, 160.0, 160.0, 159.8, and 160.1 ppm, respectively (Figure 1). It was found that the observed carbon numbers of compounds **1a**, **1b**, **2b**, **2c**, **2d**, and **2e** (13C, 16C, 14C, 20C, 16C, and 18C, respectively) were compatible with the expected carbon numbers. It was observed that two methyl signals in the ortho position on compound **1c** overlapped as single signals at 22.7 ppm. Similarly, two Ar-C signals on compound **1c** overlapped as single signals at 132.4 ppm. In addition, it was defined that the two methyl signals (2 units of CH_3) in the ortho position on compound **2a** overlapped at 22.7 ppm as a single signal as well as four Ar-C signals were overlapped at 132.0 (2 units of Ar-**C**) and 118.7 ppm (2 units of Ar-**C**) as singlets. Also, expected two methoxy carbon signals in compound **2e** were found at 56.9 (O**C**H_3) and 56.0 ppm (O**C**H_3).

Furthermore, the observed ^{1}H NMR spectra of the target compounds were found suitable for the expected values of the peaks in the aromatic and aliphatic regions (Figure 2). Moreover, the HRMS spectra results of the target compounds (**1a-1c** and **2a-2e**) were observed as $[M^+H]^+$ values (Figure 3).

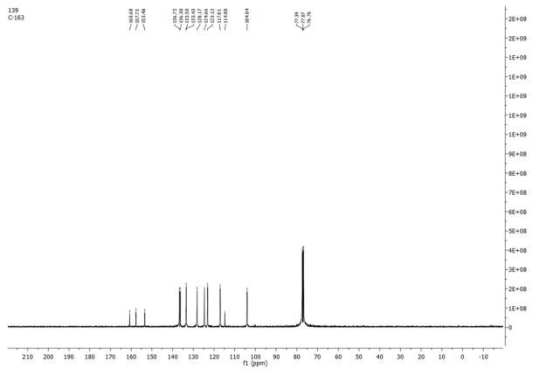

The ^{13}C NMR Spectrum ($CDCl_3$) of the 2-oxo-2*H*-chromen-4-yl thiophene-2-sulfonate (**1a**)

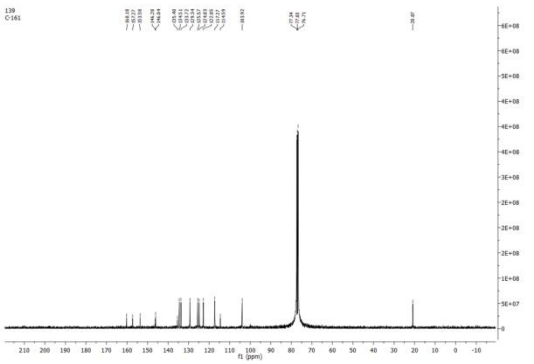

The ^{13}C NMR Spectrum ($CDCl_3$) of the 2-oxo-2*H*-chromen-4-yl 2-methyl-5-nitrobenzenesulfonate (**1b**)

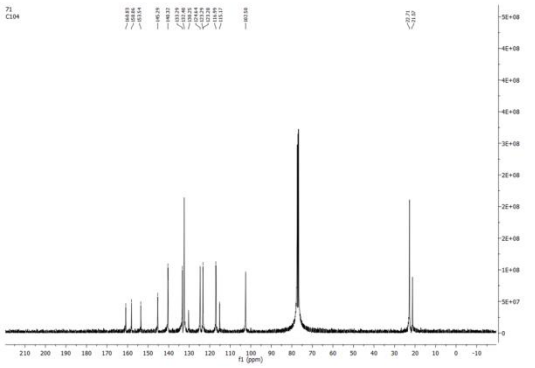

The ^{13}C NMR Spectrum ($CDCl_3$) of the 2-oxo-2*H*-chromen-4-yl 2,4,6-trimethylbenzenesulfonate (**1c**)

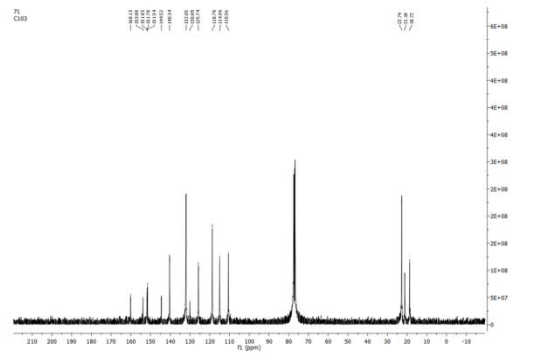

The ^{13}C NMR Spectrum ($CDCl_3$) of the 4-methyl-2-oxo-2*H*-chromen-7-yl 2,4,6-trimethylbenzenesulfonate (**2a**)

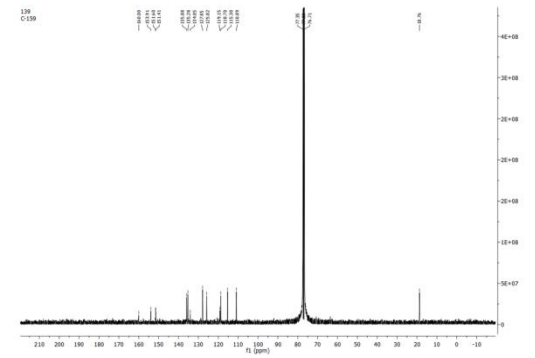

The ^{13}C NMR Spectrum ($CDCl_3$) of the 4-methyl-2-oxo-2*H*-chromen-7-yl thiophene-2-sulfonate (**2b**)

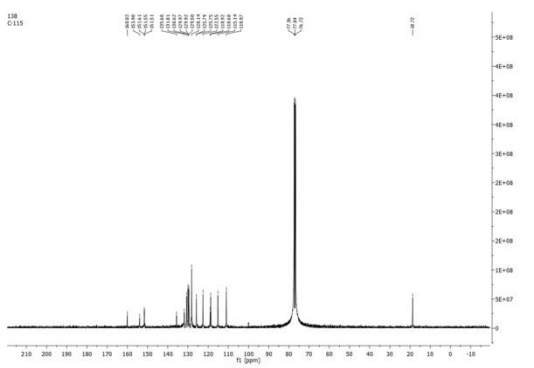

The ^{13}C NMR Spectrum ($CDCl_3$) of the 4-methyl-2-oxo-2*H*-chromen-7-yl naphthalene-2-sulfonate (**2c**)

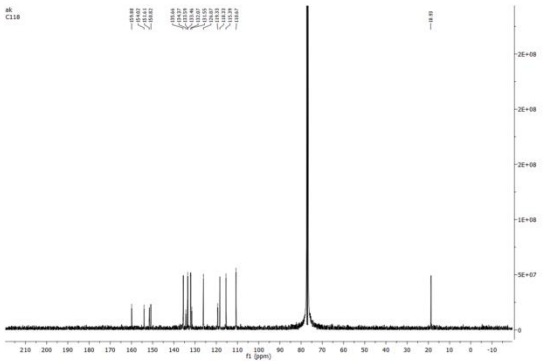

The ^{13}C NMR Spectrum ($CDCl_3$) of the 4-methyl-2-oxo-2*H*-chromen-7-yl 2,5-dichlorobenzenesulfonate (**2d**)

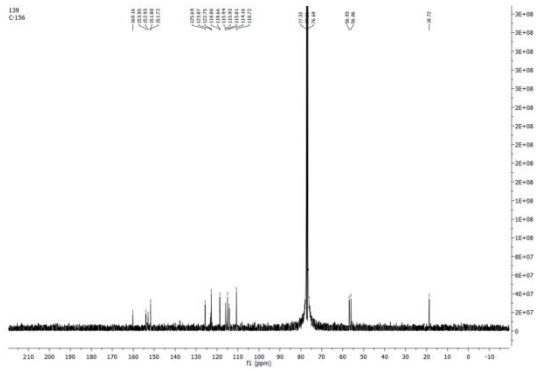

The ^{13}C NMR spectrum ($CDCl_3$) of the 4-methyl-2-oxo-2*H*-chromen-7-yl 2,5-dimethoxybenzenesulfonate (**2e**)

Figure 1. The ^{13}C NMR spectra ($CDCl_3$) of the coumarin sulfonate derivatives (**1a-1c** and **2a-2e**)

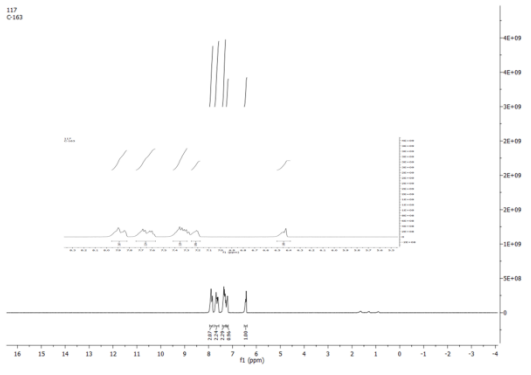

The ^{1}H NMR Spectrum ($CDCl_3$) of the 2-oxo-2*H*-chromen-4-yl thiophene-2-sulfonate (**1a**)

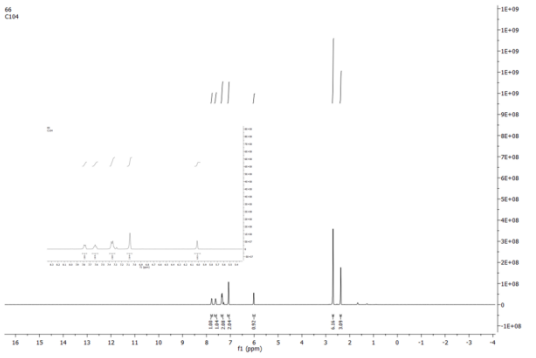

The ^{1}H NMR Spectrum ($CDCl_3$) of the 2-oxo-2*H*-chromen-4-yl 2,4,6-trimethylbenzenesulfonate (**1c**)

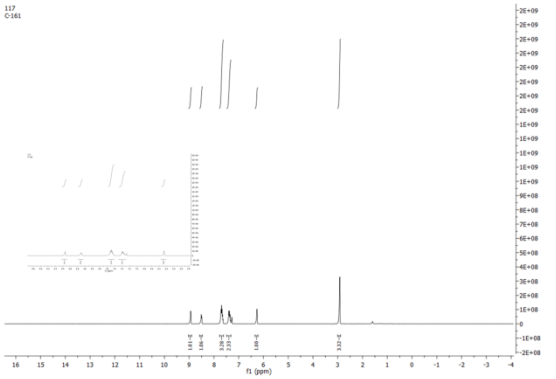

The ^{1}H NMR Spectrum ($CDCl_3$) of the 2-oxo-2*H*-chromen-4-yl 2-methyl-5-nitrobenzenesulfonate (**1b**)

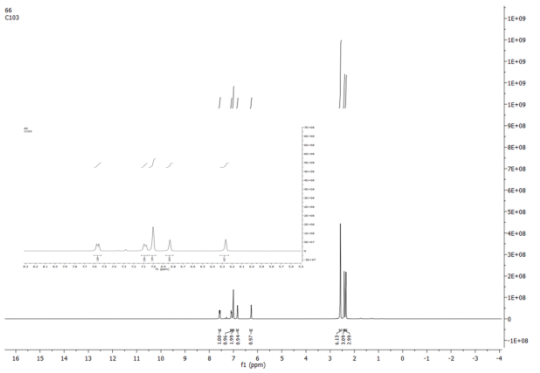

The ^{1}H NMR Spectrum ($CDCl_3$) of the 4-methyl-2-oxo-2*H*-chromen-7-yl 2,4,6-trimethylbenzenesulfonate (**2a**)

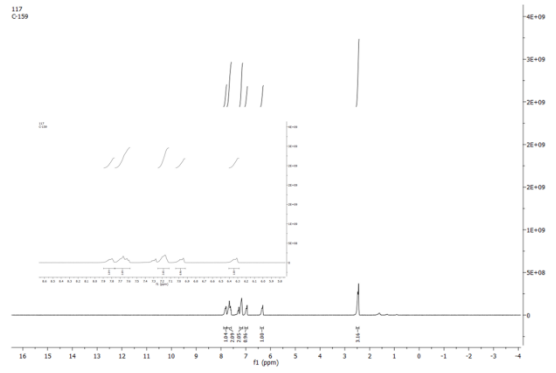

The ^{1}H NMR Spectrum ($CDCl_3$) of the 4-methyl-2-oxo-2*H*-chromen-7-yl thiophene-2-sulfonate (**2b**)

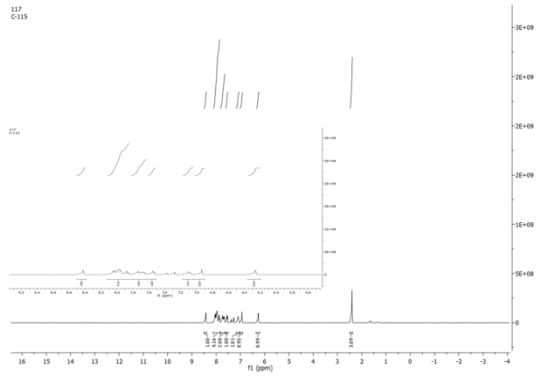

The ^{1}H NMR Spectrum ($CDCl_3$) of the 4-methyl-2-oxo-2*H*-chromen-7-yl naphthalene-2-sulfonate (**2c**)

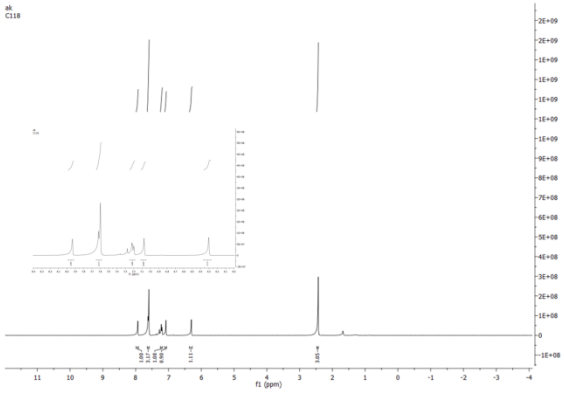

The ^{1}H NMR Spectrum ($CDCl_3$) of the 4-methyl-2-oxo-2*H*-chromen-7-yl 2,5-dichlorobenzenesulfonate (**2d**)

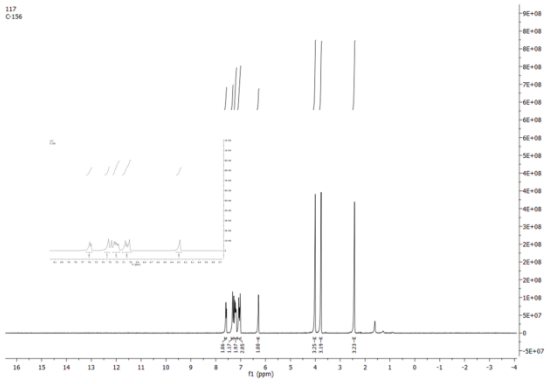

The ^{1}H NMR spectrum ($CDCl_3$) of the 4-methyl-2-oxo-2*H*-chromen-7-yl 2,5-dimethoxybenzenesulfonate (**2e**)

Figure 2. The ^{1}H NMR spectra ($CDCl_3$) of the coumarin sulfonate derivatives (**1a-1c** and **2a-2e**)

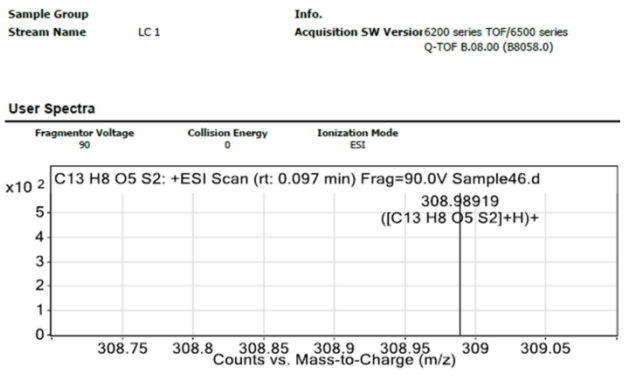

The Q-TOF Spectrum of the the 2-oxo-2*H*-chromen-4-yl thiophene-2-sulfonate (**1a**)

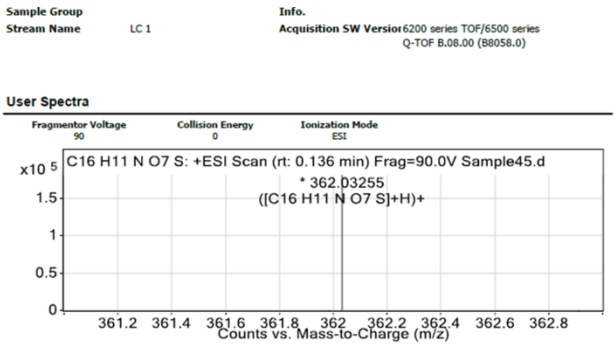

Q-TOF Spectrum of the 2-oxo-2*H*-chromen-4-yl 2-methyl-5-nitrobenzenesulfonate (**1b**)

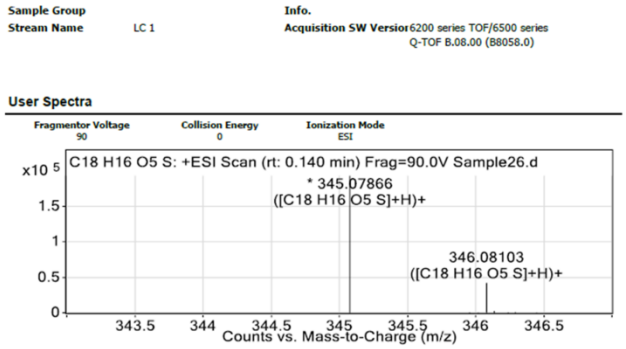

Q-TOF Spectrum of the 2-oxo-2*H*-chromen-4-yl 2,4,6-trimethylbenzenesulfonate (**1c**)

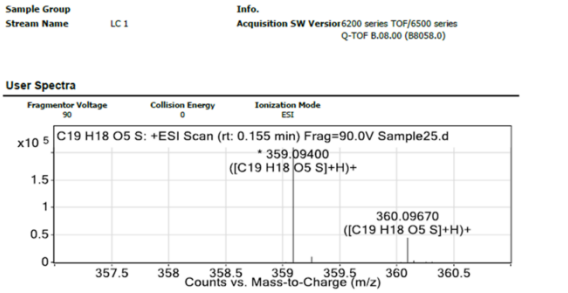

Q-TOF Spectrum of the 4-methyl-2-oxo-2*H*-chromen-7-yl 2,4,6-trimethylbenzenesulfonate (**2a**)

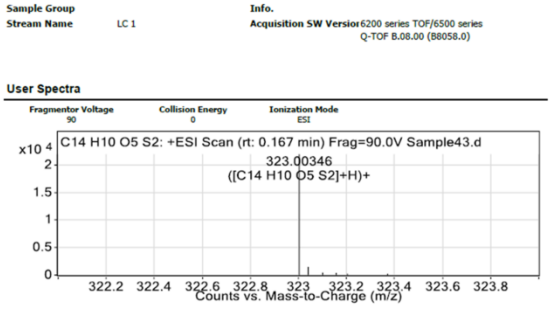

Q-TOF Spectrum of the 4-methyl-2-oxo-2*H*-chromen-7-yl thiophene-2-sulfonate (**2b**)

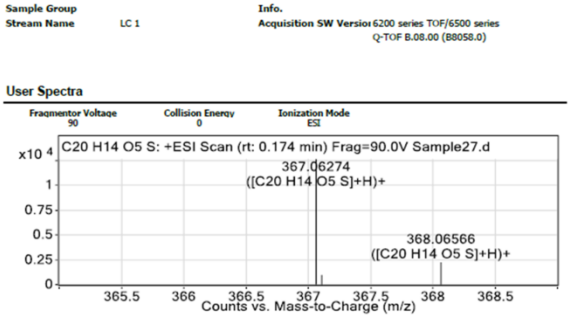

Q-TOF Spectrum of the 4-methyl-2-oxo-2*H*-chromen-7-yl naphthalene-2-sulfonate (**2c**)

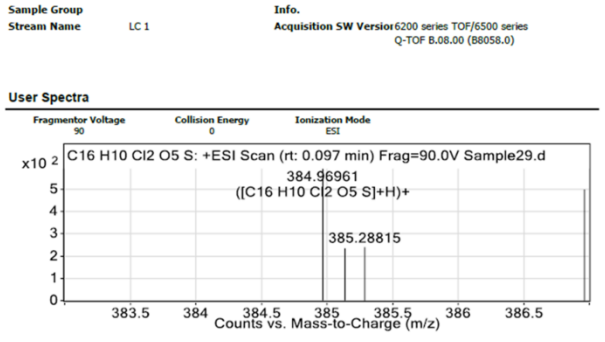

Q-TOF Spectrum of the 4-methyl-2-oxo-2*H*-chromen-7-yl 2,5-dichlorobenzenesulfonate (**2d**)

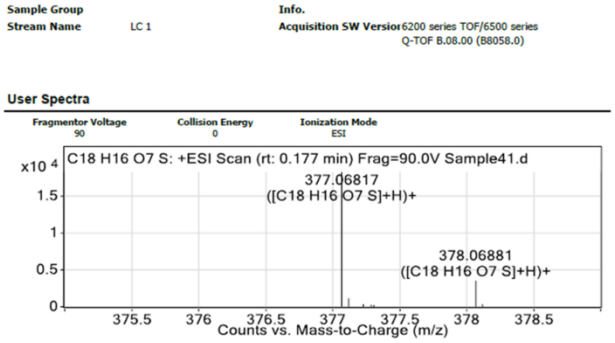

Q-TOF spectrum of the 4-methyl-2-oxo-2*H*-chromen-7-yl 2,5-dimethoxybenzenesulfonate (**2e**)

Figure 3. The Q-TOF spectra of the coumarin sulfonate derivatives (**1a-1c** and **2a-2e**)

Molecular docking studies of tyrosinase and pancreatic lipase with the coumarin sulfonate compounds

Binding affinity values were calculated to determine the effectiveness of compounds (**1a-1c** and **2a-2e**) in both tyrosinase and pancreatic lipase inhibition. The binding affinities of the coumarin sulfonate derivatives (**1a-1c** and **2a-2e**) with tyrosinase enzyme were calculated as -8.0, -7.7, -7.2, -7.1, -6.9, -7.8, -7.2, and -6.6 kcal/mol, respectively. The best affinity with tyrosinase enzyme was found with 2-oxo-2*H*-chromen-4-yl thiophene-2-sulfonate (**1a)** (-8.0 kcal/mol), (Table 1). The 2D structure and H-bond pose of the compounds showing only the best and worst binding affinity with tyrosinase were displayed in **Figure 4**.

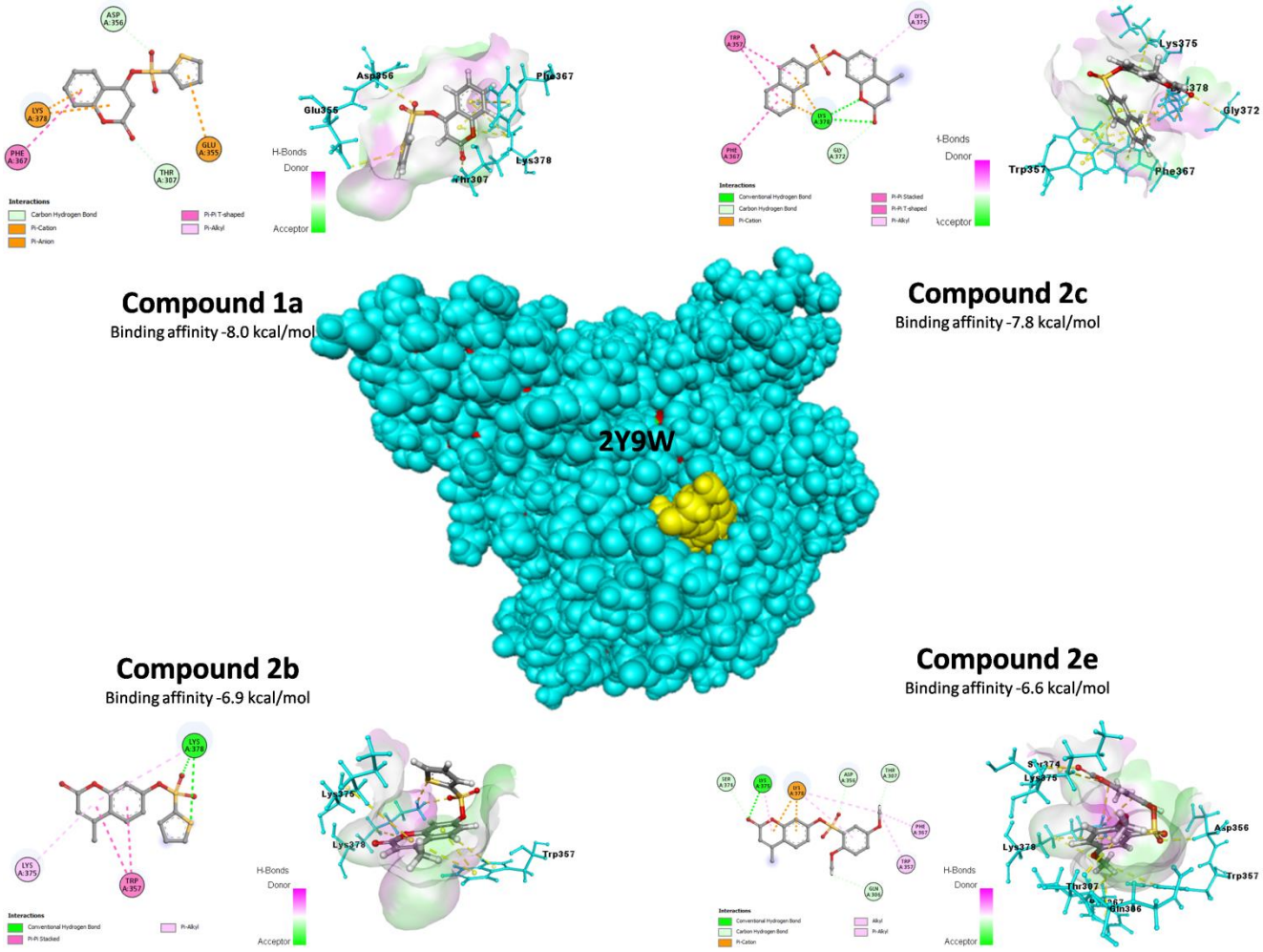

Figure 4. The 2D-structure and H-bond interaction poses of the **1a, 2b, 2c,** and **2e** with tyrosinase enzyme

The best interaction of the compound **1a** with tyrosinase was displayed as π-anion interaction (GLU A:375), π- π T-shaped interaction (PHE A:367), π-cation interaction (LYS A:378), π-alkyl interaction (LYS A: 378), and carbon hydrogen bond interactions (THR A:307 and ASP A:356). The interactions of the carbon-hydrogen bond (GLY A:372), π-cation (LYS A:378), π -π stacked (TRP A:357), π-alkyl (LYS A:375 and LYS A:378), conventional hydrogen bond (LYS A:378), and π -π T-shaped (PHE A:367) were observed on compound **2c** with tyrosinase enzyme. It was found that **1a** compound has the best binding affinity value compared to other compounds that interact with amino acids GLU A:355 and LYS A:375 like kojic acid as a standard. Compounds **2b** and **2c** were exhibited the same amino acid interaction (LYS A:375) similar to kojic acid (Korkmaz and Bursal, 2022a). In addition, GLN A:306, LYS A:375 amino acid interaction of compound **2e** with tyrosinase was

observed similar to kojic acid. Moreover, the affinity values of all compounds were calculated to be more effective than the affinity value of the standard kojic acid. All these results support these data (Table 1).

Table 1. Molecular docking interactions of tyrosinase

Compounds	Affinity (kcal/mol)	Type of Interactions	Residue Information
1a	-8.0	Carbon-Hydrogen Bond	THR A:307; ASP A:356
		π-Cation	LYS A:378
		π-Anion	GLU A:355
		π -π T-shaped	PHE A:367
		π-Alkyl	LYS A:378
2c	-7.8	Conventional Hydrogen Bond	LYS A:378
		Carbon-Hydrogen Bond	GLY A:372
		π- Cation	LYS A:378
		π -π stacked	TRP A:357
		π -π T-shaped	PHE A:367
		π-Alkyl	LYS A:375; LYS A:378
2b	-6.9	Conventional Hydrogen Bond	LYS A:378
		π -π stacked	TRP A:357
		π-Alkyl	LYS A:375; LYS A:378
2e	-6.6	Conventional Hydrogen Bond	LYS A:375
		Carbon-Hydrogen Bond	ASP A:356; SER A:374; GLN A:306; THR A:307
		π- Cation	LYS A:378
		Alkyl	LYS A:378
		π-Alkyl	TRP A:357; PHE A:367; LYS A:378; LYS A:375

Similarly, the binding affinities of the compounds (**1a-1c** and **2a-2e**) with pancreatic lipase were found at -9.0, -10.3, -10.2, -10.1, -9.1, -11.3, -9.8, and -8.8 kcal/mol, separately (Table 2). It has been observed that the compounds (**1a-1c** and **2a-2e**) have higher affinity values than the binding affinity values of orlistat (-7.1 kcal/mol), which is used as a standard for pancreatic lipase (Korkmaz and Bursal, 2022a). The best affinity with pancreatic lipase enzyme among the compounds was found for compound **2c** (-11.3 kcal/mol). The 2D structure and H-bond pose of the compounds showing only the best (**2c** and **1b**) and worst (**1a** and **2e**) binding affinity with pancreatic lipase were displayed in **Figure 5**.

The interactions of the **2c** with pancreatic lipase were determined as hydrogen bonds including carbon-hydrogen bond as ARG A:257 and conventional hydrogen bond as ARG A:257. Also, π-sulfur interaction was monitored as HIS A:264. In addition, the interaction of SER A:153 was found as an unfavorable acceptor-acceptor bond. Furthermore, π-π stacked aminoacid interactions of compound **2c** were observed PHE A:216 and TYR A:115. Moreover, the interaction of π-π T-shaped was observed as PHE A:78. Alkyl interaction was found as VAL A:260, as well as π-alkyl interactions were predicted ILE A:79, VAL A:260, and PRO A:181.

All interactions of the compounds **1a** and **1b** with pancreatic lipase were found similar to orlistat (Korkmaz and Bursal, 2022a). For example, the interactions of compound **1b** were demonstrated as SER A:153, PRO A:181, PHE A:78, TYR A:115, HIS A:264, ALA A:261, LEU A:265, PHE A:216, ARG A:257, and VAL A:260. Also, the interactions of compound **1b** were calculated as HIS A:152, SER A:153, PHE A:78, HIS A:264, PHE A:216, VAL A:260, ALA A:261, and LEU A:265. The interactions of compound **2e** were noted as SER A:153, ALA A:179, PHE A:216, ARG A:257, HIS A:264, PHE A:78, ALA A:261VAL A:260, PRO A:181, LEU A:265, TYR A:115, HIS A:152, TRP A:253, LEU A:265. It is known that the best interaction type of intermolecular is the hydrogen bond. The interactions hydrogen bond of compounds **1a, 1b,** and **2e** have been observed similar to orlistat (SER A:153). It means that these compounds have strong interactions with pancreatic lipase.

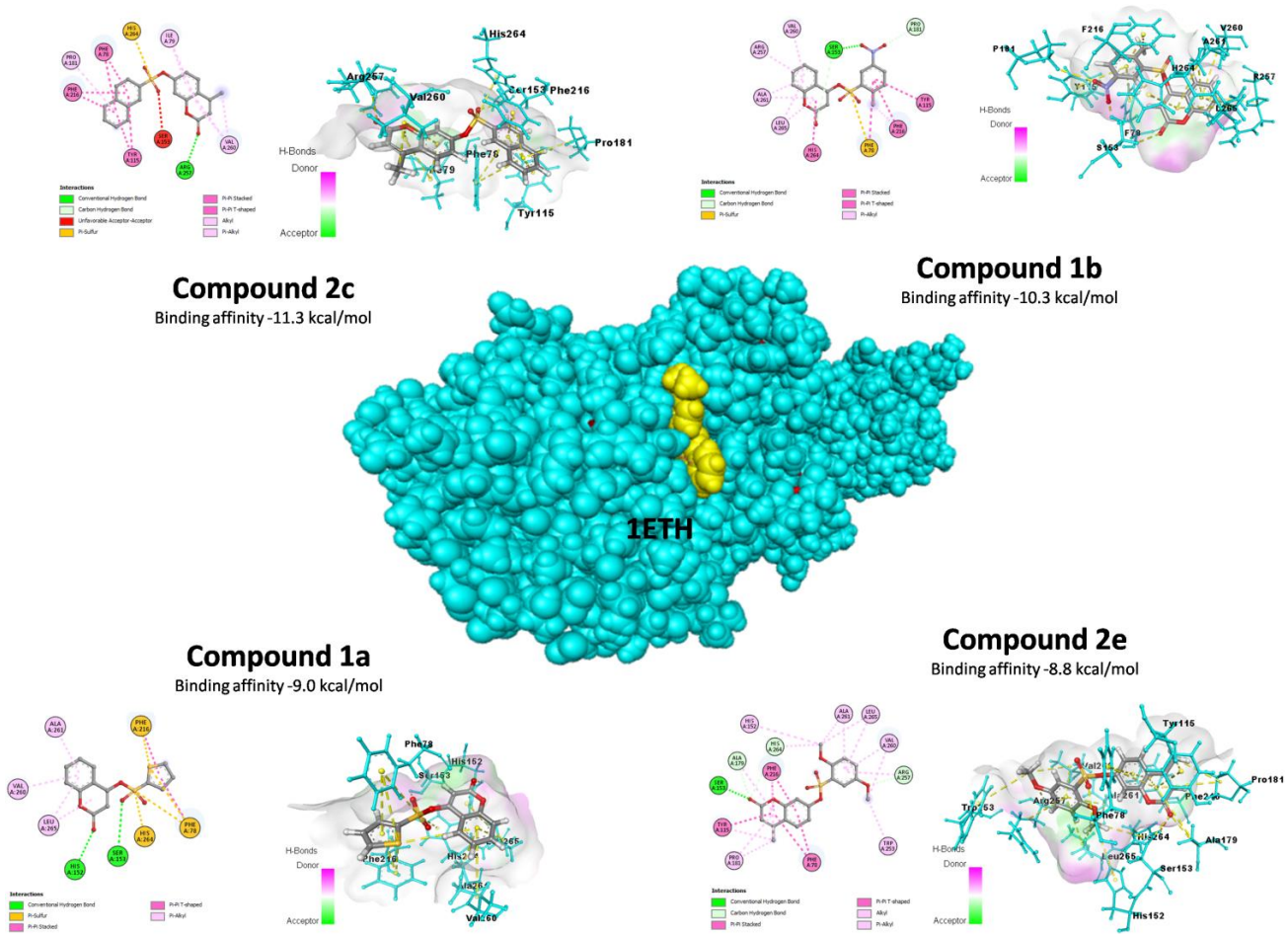

Figure 5. The 2D-structure and H-bond interaction poses of the **1a, 1b, 2c,** and **2e** with pancreatic lipase enzyme

Table 2. Molecular docking interactions of pancreatic lipase

Compounds	Affinity (kcal/mol)	Type of Interactions	Residue Information
2c	-11.3	Conventional Hydrogen Bond	ARG A:257
		Carbon-Hydrogen Bond	ARG A:257
		Unfavorable acceptor-acceptor	SER A:153
		π--Sulfur	HIS A:264
		π -π stacked	PHE A:216; TYR A:115
		π -π T-shaped	PHE A:78
		Alkyl	VAL A:260
		π-Alkyl	ILE A:79; VAL A:260; PRO A:181
1b	-10.3	Conventional Hydrogen Bond	SER A:153
		Carbon-Hydrogen Bond	SER A:153; PRO A:181
		π--Sulfur	PHE A:78
		π -π Stacked	PHE A:216; TYR A:115;HIS A:264
		π -π T-shaped	PHE A:78
		π-Alkyl	PHE A:216; ALA A:261; LEU A:265; ARG A:257; VAL A:260
1a	-9.0	Conventional Hydrogen Bond	SER A:153;HIS A:152
		π--sulfur	PHE A:78; HIS A:264; PHE A:216
		π -π stacked	PHE A:216
		π -π T-shaped	PHE A:78
		π-Alkyl	ALA A:261; LEU A:265; VAL A:260
2e	-8.8	Conventional Hydrogen Bond	SER A:153
		Carbon-Hydrogen Bond	ALA A:179; ARG A:257; HIS A:264
		π -π stacked	PHE A:216; TYR A:115
		π -π T-shaped	PHE A:78
		Alkyl	ALA A:261; LEU A:265; VAL A:260; PRO A:181
		π-Alkyl	TYR A:115; HIS A:152; PHE A:216; TRP A:253; HIS A:264;ARG A:257; VAL A:260; ALA A:261; LEU A:265; ALA A:179; PRO A:181

In silico ADMET predictions

It was investigated to define the pharmacokinetics, drug-likeness, and toxicity properties of coumarin sulfonate compounds using the preADMET and Molinspiration software (Lee, et al., 2017; Molinspiration, 2011).

The human intestinal absorption (HIA) values were calculated as >70 for all coumarin sulfonate derivatives. So, it was concluded that the HIA values of the compounds were pointed to be well absorbed (from 70% to 100%) (Oja and Maran., 2018). Caco2 values of the **1a**, **1b**, and **2b** were noted low permeability (Caco2 < 4 is low), as well as the other compounds (**1c**, **2a**, **2c**, **2d**, **2e**), were noticed with middle permeability (Caco2 = 4–70) (Li, et al., 2020). Blood-brain barrier (BBB) value of the **1b** was observed as central nervous system (CNS)-inactive (BBB > 0.40) and the other compounds (**1a**,**1c**, **2a**, **2b**, **2c**, **2d**, and **2e**) were exhibited as CNS-active (BBB < 0.40) (Chen, et al., 2021). Furthermore, skin permeability values of the coumarin sulfonate derivatives were gives an inference of good absorption by the skin (Nunes, et al., 2020).

Table 3. Drug-likeness / ADME/ toxicity prediction data of the structures

	Druglikeness / ADME/ toxicity prediction of coumarin sulfonate compounds											
	Rule of five	[a]Caco2	HIA	[b]BBB	Anes test	Carcino mouse	Carsino rat	hERG inhibition	[c]MDCK nm/s	Skin permeability	Buffer solubility (mg/L)	PPB
1a	suitable	0.9329	98.280	0.5311	mutagen	positive	negative	Low risk	27.3244	-2.21512	2152.17	100.000
1b	suitable	0.4347	93.877	0.3545	mutagen	positive	negative	Low risk	10.889	-2.02558	94.7019	100.000
1c	suitable	18.163	98.827	2.8408	mutagen	negative	negative	Medium risk	4.2006	-1.7889	685.409	100.000
2a	suitable	19.013	98.685	3.6159	non-mutagen	negative	negative	Medium risk	0.1652	-1.71019	113.336	100.000
2b	suitable	1.3714	98.646	0.92126	mutagen	positive	negative	Medium risk	10.1597	-2.0819	357.501	100.000
2c	suitable	17.503	97.741	3.17437	non-mutagen	negative	negative	Medium risk	0.13334	-1.81414	18.8756	100.000
2d	suitable	12.096	97.751	3.5325	mutagen	positive	positive	Medium risk	0.09171	-1.88244	71.0537	100.000
2e	suitable	19.483	99.276	1.2256	non-mutagen	negative	positive	Medium risk	0.09494	-2.03154	177.503	100.000

The compounds **2a, 2c,** and **2e** were determined as non-mutagen and the other compounds **1a, 1b, 2b,** and **2d** were shown to mutagen. The compounds **1c, 2a, 2c,** and **2e** were observed negative for the carcinogenicity mouse, and the other compounds **1a, 1b, 2b,** and **2d** exhibited positive. Also, the compounds were noted as negative for carcinogenicity rat except for compounds **2d** and **2e**. The hERG inhibition was determined medium risk for compounds **1c, 2a, 2b, 2c, 2d,** and **2e**. On the other hand, the hERG inhibition of compounds **1a** and **1b** were exhibited low risk. According to obtained results, the coumarin sulfonate derivatives (**1b, 1c, 2a, 2b, 2c, 2d,** and **2e**) were found low cell permeability for the Mandin Darby Canine Kidney (MDCK) except for **1a** which was medium permeability. Furthermore, it was determined that the plasma protein bind (PPB) values of the coumarin sulfonate derivatives (**1a**-**1c** and **2a**-**2e**) showed strongly bounding (Moussa, et al., 2018).

Table 4. *In silico* physicochemical properties of the coumarin sulfonate derivatives

Compound	MW	miLog	TPSA	HBA	HBD	nrotB
1a	231.12	2.85	73.59	5	0	3
1b	280.31	3.24	119.41	8	0	4
1c	290.09	4.11	73.59	5	0	3
2a	306.65	4.53	73.59	5	0	3
2b	247.68	3.28	73.59	5	0	3
2c	300.96	4.51	73.59	5	0	3
2d	284.04	4.62	73.59	5	0	3
2e	308.06	3.37	92.06	7	0	5

Topological polar surface area (TPSA) values of the coumarin sulfonate derivatives were determined at lower than 140 Å (Angstrom) (Whitty, et al., 2017). It was might be concluded to appear

drug-likeness properties thanks to the TPSA values of the compounds. Moreover, It was determined that all coumarin sulfonate derivatives were suitable for Lipinski's "Rule of five" (Table 4).

CONCLUSION

To summarise, the novel coumarin sulfonate derivatives were synthesized with mild reaction conditions and characterized (^{1}H NMR, ^{13}C NMR, and HRMS) for pancreatic lipase and as tyrosinase inhibitors *in silico* application. According to *in silico* molecular docking analyses, compounds **1a** and **2c** were exhibited more effective tyrosinase inhibition. On the other hand, compounds **1b** and **2c** were displayed the most inhibitory activities than other compounds for pancreatic lipase. Furthermore, the compounds were calculated in ADMET studies to determine pharmacological, drug-likeness, and physicochemical properties. As uncovered data results, it was observed that all compounds obeyed Lipinski's "Rule of five". Also, **1a** and **1b** were exhibited low risk for hERG inhibition. Deeply, compound **2c** having properties of the non-mutagen, negative carcinogenicity (rat and mouse), and good inhibition of pancreatic lipase and tyrosinase, has been uncovered to the fore in this study.

ACKNOWLEDGEMENTS

The author thanks DAYTAM for the 20% discount on HRMS analyses.

Conflict of Interest

The article author declare that there is no conflict of interest between them.

Author's Contributions

Adem Korkmaz carried out the design, synthesis of coumarin sulfonate compounds, analysis of the structures, written the draft, review, ADMET studies and molecular docking studies by *in silico* process.

REFERENCES

Alyar S, Şen T, Özmen ÜÖ, Alyar H, Adem Ş, Şen C, 2019. Synthesis, spectroscopic characterizations, enzyme inhibition, molecular docking study, and DFT calculations of new Schiff bases of sulfa drugs. Journal of Molecular Structure 1185: 416-424.

Arroo RR, Sari S, Barut B, Özel A, Ruparelia KC, Şöhretoğlu D, 2020. Flavones as tyrosinase inhibitors: kinetic studies in vitro and in silico. Phytochemical Analysis 31(3): 314-321.

Ashooriha M, Khoshneviszadeh M, Khoshneviszadeh M, Rafiei A, Kardan M, Yazdian-Robati R, Emami S, 2020. Kojic acid–natural product conjugates as mushroom tyrosinase inhibitors. European Journal of Medicinal Chemistry 201: 112480.

Biovia DS, 2021. Discovery studio visualizer. San Diego, CA, USA, 936.

Buldurun K, Turan N, Bursal E, Mantarcı A, Turkan F, Taslimi P, Gülçin İ, 2020. Synthesis, spectroscopic properties, crystal structures, antioxidant activities and enzyme inhibition determination of Co (II) and Fe (II) complexes of Schiff base. Research on Chemical Intermediates 46(1): 283-297.

Bursal E, Yılmaz MA, Izol E, Türkan F, Atalar MN, Murahari M, Ahmad M, 2021. Enzyme inhibitory function and phytochemical profile of Inula discoidea using in vitro and in silico methods. Biophysical Chemistry 277: 106629.

Carneiro A, Matos MJ, Uriarte E, Santana L, 2021. Trending topics on coumarin and its derivatives in 2020. Molecules 26(2): 501.

Cetin A, Bursal E, Türkan F, 2021a. 2-methylindole analogs as cholinesterases and glutathione S-transferase inhibitors: Synthesis, biological evaluation, molecular docking, and pharmacokinetic studies. Arabian Journal of Chemistry 14(12): 103449.

Cetin A, Türkan F, Bursal E, Murahari M, 2021b. Synthesis, Characterization, Enzyme Inhibitory Activity, and Molecular Docking Analysis of a New Series of Thiophene-Based Heterocyclic Compounds. Russian Journal of Organic Chemistry 57(4): 598-604.

Chen W, Yao S, Wan J, Tian Y, Huang L, Wang S, Zhang X, 2021. BBB-crossing adeno-associated virus vector: An excellent gene delivery tool for CNS disease treatment. Journal of Controlled Release 333: 129-138.

Dorababu A, 2022. Pharmacological report of recently designed multifunctional coumarin and coumarin–heterocycle derivatives. Archiv der Pharmazie 355(2): 2100345.

El-Gamal MI, Oh CH, 2014. Synthesis, in vitro antiproliferative activity, and in silico studies of fused tricyclic coumarin sulfonate derivatives. European Journal of Medicinal Chemistry 84: 68-76.

Hanwell MD, Curtis DE, Lonie DC, Vandermeersch T, Zurek E, Hutchison GR, 2012. Avogadro: an advanced semantic chemical editor, visualization, and analysis platform. Journal of cheminformatics 4(1): 1-17.

Hariri R, Saeedi M, Akbarzadeh T, 2021. Naturally occurring and synthetic peptides: Efficient tyrosinase inhibitors. Journal of Peptide Science 27(7): e3329.

Huo PC, Hu Q, Shu S, Zhou QH, He RJ, Hou J, Ge GB, 2021. Design, synthesis and biological evaluation of novel chalcone-like compounds as potent and reversible pancreatic lipase inhibitors. Bioorganic & Medicinal Chemistry 29: 115853.

Iqbal J, El-Gamal MI, Ejaz SA, Lecka J, Sévigny J, Oh CH, 2018. Tricyclic coumarin sulphonate derivatives with alkaline phosphatase inhibitory effects: In vitro and docking studies. Journal of enzyme inhibition and medicinal chemistry 33(1): 479-484.

Korkmaz A, Bursal E, 2022a. Benzothiazole Sulfonate Derivatives Bearing Azomethine: Synthesis, Characterization, Enzyme Inhibition, and Molecular Docking Study. Journal of Molecular Structure 1257: 132641.

Korkmaz A, Bursal E, 2022b. An in vitro and in silico study on the synthesis and characterization of novel bis (sulfonate) derivatives as tyrosinase and pancreatic lipase inhibitors. Journal of Molecular Structure 1259: 132734.

Lee SK, Kang Y, Chang GS, Lee IH, Park SH, Park J, 2017. Bioinformatics and Molecular Design Research Center. Yonsei University, Seoul https://preadmet. bmdrc. kr.

Li Y, Xu Y, Pan C, Ren Z, Yang X, 2020. TRIF is essential for the anti-inflammatory effects of Astragalus polysaccharides on LPS-infected Caco2 cells. International Journal of Biological Macromolecules 159: 832-838.

Li Z, Kong D, Liu Y, Li M, 2022. Pharmacological perspectives and molecular mechanisms of coumarin derivatives against virus disease. Genes & Diseases 9(1): 80-94.

Molinspiration C, 2011. Calculation of molecular properties and bioactivity score. http://www. molinspiration. com/cgi-bin/properties.

Moussa G, Alaaeddine R, Alaeddine LM, Nassra R, Belal AS, Ismail A, Hazzaa A, 2018. Novel click modifiable thioquinazolinones as anti-inflammatory agents: Design, synthesis, biological evaluation and docking study. European journal of medicinal chemistry 144: 635-650.

Nune, AMV, de Andrade FDCP, Filgueiras LA, de Carvalho Maia OA, Cunha RL, Rodezno SV, Mendes AN, 2020. preADMET analysis and clinical aspects of dogs treated with the Organotellurium compound RF07: A possible control for canine visceral leishmaniasis?. Environmental Toxicology and Pharmacology 80: 103470.

Oja M, Maran U, 2018. pH-permeability profiles for drug substances: Experimental detection, comparison with human intestinal absorption and modelling. European Journal of Pharmaceutical Sciences 123: 429-440.

Pettersen EF, Goddard TD, Huang CC, Couch GS, Greenblatt DM, Meng EC, Ferrin TE, 2004. UCSF Chimera—a visualization system for exploratory research and analysis. Journal of computational chemistry 25(13): 1605-1612.

Salar U, Khan KM, Jabeen A, Faheem A, Fakhri MI, Saad SM, Hameed A, 2016. Coumarin sulfonates: As potential leads for ROS inhibition. Bioorganic chemistry 69: 37-47.

Schrodinger, L. L. C. 2021. The PyMOL molecular graphics system. Version, 2(5): 1.

Sultana R, Alashi AM, Islam K, Saifullah M, Haque CE, Aluko RE, 2020. Inhibitory activities of Polyphenolic extracts of Bangladeshi vegetables against α-amylase, α-glucosidase, pancreatic lipase, renin, and angiotensin-converting enzyme. Foods 9(7): 844.

Taslimi P, Türkan F, Cetin A, Burhan H, Karaman M, Bildirici I, Şen F, 2019. Pyrazole [3, 4-d] pyridazine derivatives: Molecular docking and explore of acetylcholinesterase and carbonic anhydrase enzymes inhibitors as anticholinergics potentials. Bioorganic Chemistry 92: 103213.

Tolba M, El-Dean A, Geies A, Radwan S, Zaki R, Sayed M, Abdel-Raheem S, 2022. An overview on synthesis and reactions of coumarin based compounds. Current Chemistry Letters 11(1): 29-42.

Trott O, Olson AJ, 2009. Software news and update AutoDock Vina: improving the speed and accuracy of docking with a new scoring function. Efficient Optimization, and Multithreading. Journal of computational chemistry 31: 455-461.

Turkan F, Çetin A, Taslimi P, Karaman M, Gulçin İ, 2019. Synthesis, biological evaluation and molecular docking of novel pyrazole derivatives as potent carbonic anhydrase and acetylcholinesterase inhibitors. Bioorganic chemistry 86: 420-427.

Whitty A, Viarengo LA, Zhong M, 2017. Progress towards the broad use of non-peptide synthetic macrocycles in drug discovery. Organic & Biomolecular Chemistry 15(37): 7729-7735.

Xu Z, Chen Q, Zhang Y, Liang C, 2021. Coumarin-based derivatives with potential anti-HIV activity. Fitoterapia 150: 104863.

Zhang Y, Fu X, Yan Y, Liu J, 2020. Microwave-assisted synthesis and biological evaluation of new thiazolylhydrazone derivatives as tyrosinase inhibitors and antioxidants. Journal of Heterocyclic Chemistry 57(3): 991-1002.